Available online at www.CivileJournal.org

# Civil Engineering Journal

(E-ISSN: 2476-3055; ISSN: 2676-6957)

Vol. 12, No. 01, January, 2026

# Mechanical Properties and Structural Behavior of Sustainable Ferrock Concrete for Green Construction Applications

Samy Elbialy [1, 2*], I. Alhoutary [2], Ahmed Gouda [3], Amr M. N. Ibrahim [1], Wael Ibrahim [1], Amal Hassanin Ibrahim [1], Waleed Abd-Allah [1]

[1] *Department of Civil Engineering, Faculty of Engineering at Mataria, Helwan University, Cairo 11718, Egypt.*

[2] *College of Engineering and Design, Kingdom University, P.O. Box 40434, Bahrain.*

[3] *Department of Civil and Environmental Engineering, Faculty of Engineering, King Abdulaziz University (KAU), Jeddah, Saudi Arabia.*

Received 26 October 2025; Revised 21 December 2025; Accepted 27 December 2025; Published 01 January 2026

**Abstract**

This study aims to develop a sustainable alternative to Ordinary Portland Cement (OPC) by investigating the mechanical and structural properties of Ferrock concrete, an iron carbonate-based binder composed largely of industrial by-products. An experimental program was conducted, testing over 114 concrete cubes, 18 cylinders, and 6 full-scale reinforced concrete beams with Ferrock replacing OPC at 5%, 10%, 15%, 20%, and 25% by weight. The results demonstrate that a 15% replacement ratio yields a 25% increase in 28-day compressive strength, while splitting tensile strength improves consistently with Ferrock content. Most notably, reinforced beams with 20% Ferrock exhibited up to a 33% increase in flexural capacity, with failure modes shifting toward more ductile behavior and experimental capacities exceeding predictions from ACI 318, CSA A23.3, and Eurocode 2 by up to 62%. This research confirms that Ferrock is not only a carbon-negative material but also a technically superior partial replacement for OPC, offering enhanced strength, ductility, and structural performance for green construction applications.

*Keywords:* Ferrock; Sustainable Concrete; Cement Replacement; Flexural Behavior; Reinforced Concrete Beams; Mechanical Properties; Carbon-Negative Material; Experimental Investigation.

## 1. Introduction

The global construction industry is a cornerstone of economic development, yet it remains one of the largest consumers of natural resources and a significant contributor to environmental degradation. Concrete, as the world's most consumed manufactured material, relies on Ordinary Portland Cement (OPC) as its primary binder. OPC production is responsible for approximately 8–10% of global anthropogenic carbon dioxide ($CO_2$) emissions [1]. This substantial impact stems from the calcination of limestone and the combustion of fossil fuels in cement kilns, driving the urgent search for sustainable binder alternatives as a paramount challenge in modern civil engineering [2, 3]. Consequently, extensive research into green concrete technologies aims to reduce this carbon footprint while preserving or enhancing mechanical performance and durability [4, 5].

A prevalent strategy involves partially replacing OPC with industrial by-products such as fly ash, silica fume, ground granulated blast-furnace slag (GGBS), and metakaolin to reduce the clinker factor [6, 7]. Further innovations include

* Corresponding author: s.bialy@ku.edu.bh

https://doi.org/10.28991/CEJ-2026-012-01-012

ultra-high-performance and geopolymer concretes, with studies optimizing mix designs for improved sustainability and performance [8, 9]. Alkali-activated binders (geopolymers), for instance, achieve major emission reductions by eliminating Portland cement clinker, though their environmental footprint is often linked to alkaline activator production and may involve thermal curing [8, 9]. A more transformative approach focuses on binders that are not merely less harmful but actively beneficial by sequestering $CO_2$ during curing.

Ferrock represents a groundbreaking development within this category. As an iron-based binder composed largely of recycled steel dust, its curing process involves a chemical reaction with $CO_2$ to form stable iron carbonates. This reaction hardens the matrix while permanently sequestering the greenhouse gas [10, 11]. Consequently, Ferrock achieves a "carbon-negative" status, absorbing more $CO_2$ than is emitted during its production [12]. Life Cycle Assessment (LCA) studies confirm its significantly lower environmental impact compared to OPC [13, 14]. Unlike some alkali-activated systems, Ferrock's carbonation curing proceeds under ambient conditions, offering a passive, energy-efficient sequestration pathway that directly converts $CO_2$ into a structural binder. This presents a distinct potential advantage in net carbon efficiency, particularly when materials are sourced and processed locally.

Initial investigations into Ferrock have reported promising material-level properties. Studies on paste and mortar indicate superior flexural strength and fracture toughness, attributed to its dense iron carbonate microstructure [10, 15]. Its notable resistance to acid and saltwater corrosion further suggests strong durability characteristics [16]. However, a significant gap persists in the published literature. While research has examined its paste morphology, carbonation mechanism, and mortar properties [10, 11, 17, 18], investigations into its application in full-scale structural elements are lacking. This gap becomes especially apparent when contrasted with recent, high-impact research on other sustainable concretes—such as geopolymers [8, 9] and modified Ferrock systems [19, 20]—which have advanced to detailed evaluations of reinforced concrete (RC) beams, slabs, and structural durability [8, 9, 18-20]. The fundamental structural behavior of reinforced Ferrock concrete beams, including their cracking patterns, load-deflection response, ultimate moment capacity, and failure modes, remains largely undocumented. Bridging this gap is critical, as a thorough understanding of structural performance is essential for developing practical design guidelines and facilitating industry adoption. Recent studies on novel sustainable concretes underscore the importance of such full-scale validation [19, 20].

The experimental rationale for this work integrates principles from composite material science and structural concrete mechanics. The core hypothesis posits that the iron carbonate ($FeCO_3$) formed during Ferrock's carbonation curing serves as pervasive micro-reinforcement within the cementitious matrix. This microstructural modification is anticipated to enhance the material's fracture resistance by impeding crack propagation through deflection and bridging mechanisms, thereby elevating tensile strength and mitigating brittleness [15, 19]. Structurally, these enhancements are expected to manifest in RC beams through delayed cracking, refined crack distributions that improve post-cracking stiffness, and increased ultimate moment capacity resulting from synergistic improvements in both compressive and tensile zones. The sequential experimental design—first quantifying fundamental material properties and then evaluating full-scale structural members—directly tests this hypothesis, providing a rigorous link between sustainable material modification and demonstrable structural performance gains.

This study aims to comprehensively address this research gap through a detailed experimental investigation of the mechanical and structural properties of Ferrock concrete. The primary objective is to evaluate its viability as a partial OPC replacement in load-bearing applications. The research program was designed first to establish the fundamental mechanical properties (compressive and tensile strength) of concrete mixes with varying Ferrock percentages. Subsequently, the core of the study involves testing and analyzing the flexural behavior of full-scale RC-beams fabricated with these mixes. The specific objectives are to: (1) determine the optimal Ferrock-to-cement replacement ratio for enhanced strength, (2) characterize the load-deflection response and failure mechanisms of Ferrock RC-beams, and (3) provide a comparative analysis against conventional OPC concrete and code predictions to quantify the structural benefits of this sustainable alternative.

The remainder of this paper is structured as follows: Section 2 details the experimental program, including materials, mix design, and testing protocols for both material specimens and full-scale beams. Section 3 presents and discusses the results from the mechanical property tests (Phase I) and the structural beam tests (Phase II). Section 4 summarizes the main conclusions drawn from the study. Finally, acknowledgments and references are provided.

## 2. Experimental Work

The research program was designed as two consecutive phases to build a complete profile of Ferrock concrete, progressing from its basic material characteristics to its behavior in structural applications. The first phase concentrated on the micro-scale, analyzing the component materials and evaluating the hardened mechanical properties of different Ferrock-concrete blends. The second phase utilized these foundational material insights to explore macro-scale performance through the flexural testing of full-scale RC- beams. This approach yielded essential information regarding structural application, failure modes, and load-bearing capacity. The sequence of the experimental program is outlined in Figure 1.

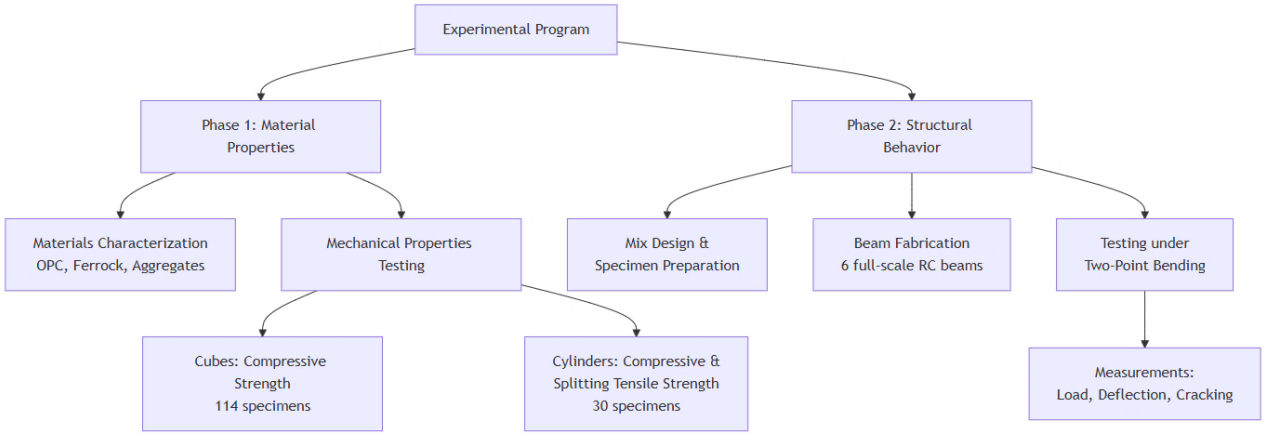


**Figure 1. Flowchart of the experimental program**

## 2.1. Properties of Constituent Materials and Mix Formulation

### 2.1.1. Material Specifications and Sourcing

Materials conforming to international standards were used throughout the investigation to guarantee consistency and reliable results. Ordinary Portland Cement (OPC) of grades 42.5N and 52.5N served as the primary binder, meeting the requirements of ES 4756/1-2013 and EN 197-1 specifications [21, 22]. The novel binder, Ferrock, was prepared according to the formulation developed by Das et al. [11]. This proprietary mixture contains 60% reclaimed iron powder—a by-product of industrial shot-blasting with a median particle size of 19.03 µm—along with 20% Class F fly ash (ASTM C618 [23]), 10% finely ground limestone (median particle size 0.7 µm, ASTM C568 [24]), 8% metakaolin (ASTM C618 [23]), and 2% oxalic acid as a carbonation catalyst [12]. In this blend, the high iron content supplies the necessary reactant for iron carbonate ($FeCO_3$) formation. Fly ash and metakaolin enhance particle packing density and contribute supplementary pozzolanic activity, while limestone functions as a micro-filler to refine the matrix. Oxalic acid promotes faster carbonation kinetics. Inert aggregates consisted of natural siliceous sand (specific gravity 2.62, fineness modulus 3.35) and coarse crushed dolomite (sizes 1 & 2; specific gravity 2.6). A high-range water-reducing superplasticizer—either ADDICRETE BVF (ASTM C494 Type F [25]) or Sikament 163M (BS 5075 Part 3 [26])—was added to maintain suitable workability across mixtures with different water requirements. The full material composition, including all binders, aggregates, and chemical admixtures, is illustrated in Figure 2. Aggregate physical properties are provided in Table 1. For reinforcement, high-tensile deformed steel bars (yield strength, $fy$ = 400 MPa) were used as longitudinal reinforcement, and mild steel bars ($fy$ = 300 MPa) served as shear stirrups.

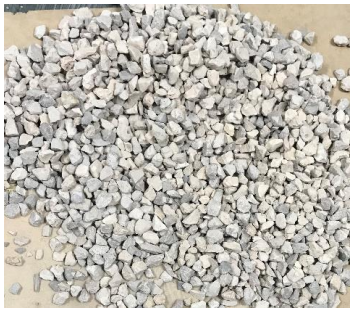

Coarse aggregates

Fine aggregates

Steel Powder

Fly Ash Class F

Metakaolin

Limestone


Oxalic Acid

Ferrock, After Mixing All the Components

**Figure 2. Ferrock Components**

**Table 1. Physical Properties of Fine and Coarse Aggregates**

| Property | Standard | Fine aggregate (Sand) | Coarse aggregate (Dolomite) |
|---|---|---|---|
| Specific gravity | ASTM C127 C128 | 2.62 | 2.60 |
| Fineness modulus | ASTM C136 | 3.35 | 6.82 |
| Water absorption (%) | ASTM C127 | 1.20 | 1.00 |
| Bulk density (kg/m³) | ASTM C29 | 1680 | 1620 |
| Max. aggregate Size (mm) | - | 4.75 | 20 |

### 2.1.2. Concrete Proportioning and Mixture Design

An iterative trial-batch process was employed to develop the concrete mix design. Initial attempts to use Ferrock as a complete cement replacement (100%) proved unworkable for structural applications. These preliminary mixtures displayed inadequate cohesion, poor workability, and an excessively rapid set, which hindered proper compaction and led to incomplete specimen formation. This outcome necessitated a shift in strategy, adopting Ferrock as a partial replacement for cement. To establish a workable baseline, a minimum of 5% OPC by weight was included to provide essential initial cohesion and regulate hydration. Subsequent testing phases systematically evaluated Ferrock by replacing cement at five incremental levels: 5%, 10%, 15%, 20%, and 25% by weight, alongside a conventional 0% control mix. This approach allowed for a precise assessment of Ferrock's influence while maintaining the necessary workability for fabricating testable structural elements. The water-to-binder (w/b) ratio—where the binder comprises the total mass of cement and Ferrock—was controlled within a range of 0.32 to 0.54 across the different mixes. Superplasticizer dosage was varied between 2% and 3% by weight of cement to attain a target slump of 80–100 mm, ensuring adequate workability for placement and consolidation. The exact proportions for one cubic meter of concrete for each mix design are provided in Table 2.

**Table 2. Final Mix Proportions per Cubic Meter of Concrete**

| Mix ID | Cement (kg) | Cement Grade | Ferrock (%) | Water-to-binder (w/b) ratio | Coarse agg. (kg) | Fine agg. (kg) | Super-plasticizer (kg) |
|---|---|---|---|---|---|---|---|
| M-0.0 (Control) | 350 | 42.5 | 0.0 | 0.49 | 1180 | 680 | 0.00 |
| M-5.0 (5% F) | | | 5.0 | 0.45 | | | 7.00 |
| M-10 (10% F) | | | 10 | 0.41 | | | 8.80 |
| M-15 (15% F) | | | 15 | 0.35 | | | 8.80 |
| M-20 (20% F) | | | 20 | 0.38 | | | 7.00 |
| M-25 (25% F) | | 52.5 | 25 | 0.40 | | | 10.5 |

## 2.2. Specimen Design and Testing Protocol

### 2.2.1. Phase 1: Evaluation of Mechanical Properties

Phase I implemented a detailed testing program to quantify the essential mechanical properties of the concrete mixtures. In total, 114 standard 150 mm cubes were cast to assess compressive strength development after 7 and 28 days of curing, following established testing protocols [24]. Each mixture was represented by 19 cubes. The mix identification system uses a two-part code: the letter 'M' signifies 'mix,' followed by a number corresponding to the percentage of cement replaced by Ferrock by weight. Additionally, 18 standard cylinders (150 mm diameter × 300 mm height) were produced to evaluate splitting tensile strength at 28 days, providing further insight into the material's response to different stress states [27]. The complete testing schedule for Phase I is outlined in Table 3 and illustrated in Figure 3-a.

**Table 3. Testing Schedule for Phase 1 (Material Properties)**

| Specimen type | Standard | Number of specimens | Test age (days) | Key parameter measured |
|---|---|---|---|---|
| Cube (150 mm) | ASTM C39 / EN 12390-3 | 114 (19 per mix) | 7, 28 | Compressive Strength ($f_{cu}$) |
| Cylinder (150×300 mm) | ASTM C496 | 18 (3 per mix) | 28 | Splitting Tensile Strength ($f_{ct}$) |

(a) Samples for Compressive and Tensile Strengths

(b) Plywood Form of the Beams

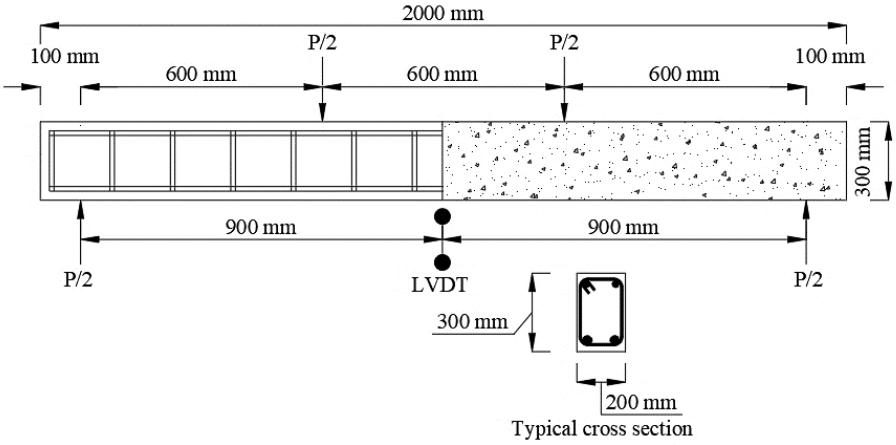


(c) Cross Section of the Beams

**Figure 3. Specimens Details**

### 2.2.2. Phase 2: Structural Performance Assessment

Phase II advanced the investigation from material characterization to structural assessment by fabricating and testing six full-scale RC- beams. To ensure that variations in concrete mixture were the sole influencing factor, all beams were constructed with identical geometry and reinforcement detailing. Each beam measured 2000 mm in length, 200 mm in width, and 400 mm in depth. The reinforcement was specifically configured to promote flexural failure, consisting of two 16 mm high-tensile steel bars at the bottom (tension zone) and two 10 mm bars at the top (compression zone). Shear reinforcement, comprising 8 mm diameter mild steel stirrups spaced at 100 mm centers along the entire span, was included to preclude premature shear failure. The experimental program, outlined in Table 4 and depicted in Figure 3-b and (c), included one beam for each designated Ferrock replacement percentage.

**Table 4. Test Matrix for Reinforced Concrete Beams (Phase 2)**

| Beam ID | Ferrock Replacement (%) | Concrete Grade Target |
|---|---|---|
| B-0.0-35 | 0 (Control) | C35 |
| B-5.0-35 | 5 | |
| B-10-35 | 10 | |
| B-15-40 | 15 | C40 |
| B-20-35 | 20 | C35 |
| B-25-30 | 25 | C30 |

Each beam is identified using a three-part code that concisely conveys its key attributes. The initial character, "B," designates the specimen as a beam. The following character specifies the percentage of Ferrock by weight within the concrete mix. The final character denotes the target concrete strength grade employed in the beam's construction. This structured naming convention facilitates rapid identification and straightforward comparison of beam compositions in structural documentation and analysis.

## 2.3. Instrumentation and Experimental Procedures

### 2.3.1. Phase 1: Standardized Material Testing Procedures

All material specimens were fabricated under controlled laboratory conditions. Fresh concrete was prepared in a drum mixer, placed into steel molds in two successive layers, and compacted on a vibrating table to ensure thorough consolidation and eliminate entrapped air. Following a 24-hour initial cure in the molds at a controlled environment (23±2°C and >95% relative humidity), the specimens were demolded and subsequently submerged in a water-curing tank maintained at 23±2°C until reaching their specified testing age. Compressive tests on both cubes and cylinders were conducted using a servo-controlled universal testing machine (UTM) with a 3000 kN capacity, as shown in Figure 4. A central load was applied to the specimen's bearing surface at a continuous rate of 0.6 MPa/s until failure, adhering to standardized procedures [27, 28]. Splitting tensile strength was determined by applying a compressive line load along the length of a horizontally positioned cylinder placed between two plywood bearing strips. This configuration induces a nearly uniform tensile stress across the vertical diameter, resulting in the characteristic splitting failure mode described in the standard [29].


**Figure 4. Universal Testing Machine**

### 2.3.2. Phase 2: Flexural Testing of Reinforced Beams

Beam testing commenced after a minimum 28-day curing period. Each beam was installed in a loading frame as a simply supported element with a clear span of 1800 mm, illustrated in Figure 5. A two-point loading configuration was implemented using a 1000 kN hydraulic jack and a rigid spreader I-beam to apply two concentrated loads spaced 600 mm apart. This arrangement produced a region of pure bending moment—with zero shear—between the load points. A calibrated load cell connected to a data acquisition system provided precise measurement of the applied force. Structural response was tracked with three Linear Variable Differential Transformers (LVDTs) with 0.01 mm accuracy, positioned to capture deflections at mid-span, where maximum deflection occurs. Loading proceeded in force-controlled increments of approximately 5 kN. At each increment, the test was paused to carefully document the formation, propagation, and width of all flexural and shear cracks using a crack microscope. Testing continued until a pronounced decline in load-carrying capacity signaled ultimate failure, enabling the observation of failure modes and the compilation of complete load-deflection data for every beam.

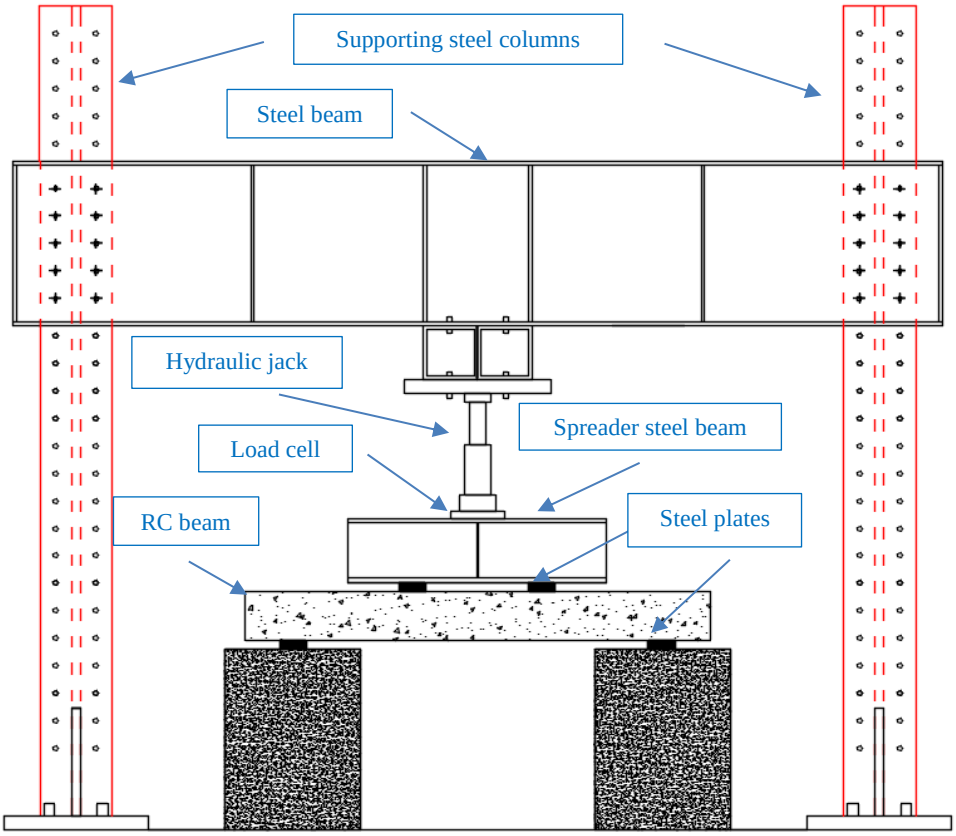


(a) Schematic drawing

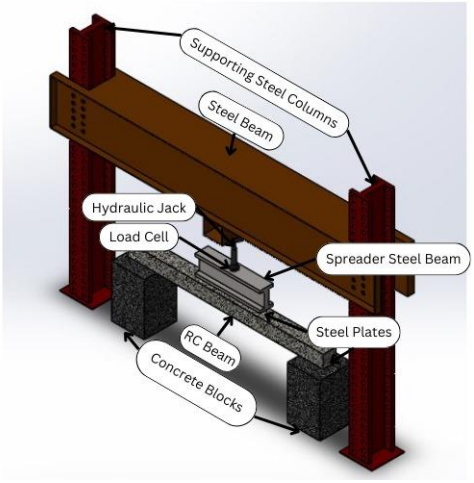


(b) 3D

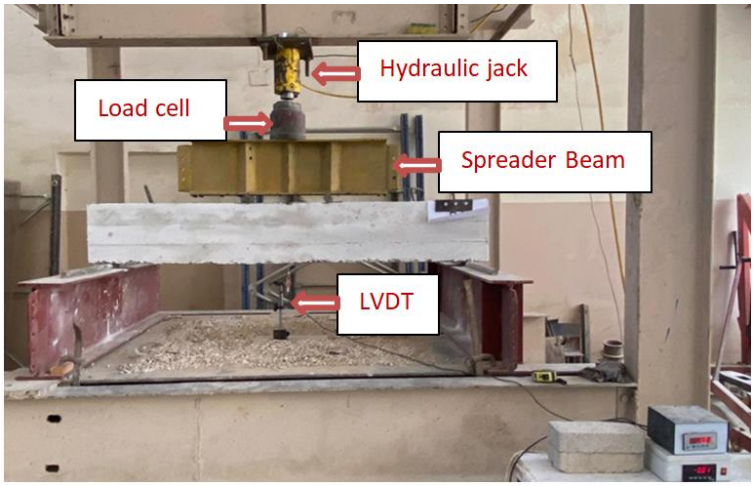


(c) Actual

**Figure 5. Test Setup for the Beams**

## 3. Results and Discussion

### 3.1. Phase I

The sections that follow provide a comprehensive analysis of the compressive and tensile strength data obtained in Phase I of this investigation. The results illustrate the influence of different Ferrock percentages on the fundamental mechanical response of concrete, revealing clear trends in strength progression, failure modes, and microstructural interaction. This evaluation offers essential insights for determining the optimal replacement level and understanding the functional behavior of Ferrock as a sustainable substitute for traditional cement-based materials.

#### 3.1.1. Compressive Strength Analysis

The results presented in Table 5 indicate a complex, non-linear relationship between Ferrock content and concrete strength development. The performance across the six mixtures defines three distinct zones, each governed by a predominant physical or chemical mechanism.

**Table 5. Compressive Strength Test Results**

| Mix ID | Ferrock (%) | 7-Day strength (MPa) | 28-Day strength (MPa) | Strength gain (7 to 28 days) | Strength increase vs. B1 | Strength Efficiency Index (SEI) |
|---|---|---|---|---|---|---|
| M-0.0 | 0 (Control) | 21.4 | 37.0 | +15.6 (+73%) | Baseline (0%) | 1.00 |
| M-5.0 | 5 | 24.0 | 38.9 | +14.9 (+62%) | +5.1% | 1.05 |
| M-10 | 10 | 25.1 | 39.6 | +14.5 (+58%) | +7.0% | 1.07 |
| M-15 | 15 | 26.6 | 46.4 | +19.8 (+74%) | +25.4% | 1.25 |
| M-20 | 20 | 22.1 | 37.9 | +15.8 (+71%) | +2.4% | 1.02 |
| M-25 | 25 | 20.4 | 35.0 | +14.6 (+72%) | -5.4% | 0.95 |

* SEI = (28-day strength of Mix) / (28-day strength of Control). An SEI > 1 indicates superior.

Zone 1: Marginal Enhancement (Mixes M-5.0 and M-10). These initial mixtures exhibit a positive, though modest, improvement relative to the control mix (M-0.0). The 28‑day cube strength rose by 1.9 MPa (5.1%) for M‑5.0 and by 2.6 MPa (7.0%) for M‑10. This early enhancement is ascribed mainly to a physical filler effect and the initiation of weak pozzolanic reactions. The fine particles of fly ash and metakaolin contained in the Ferrock blend, being smaller than cement grains, fill microscopic voids between cement and aggregate particles. This reduces overall porosity and produces a denser, more compact matrix that demands greater energy to compress and fail [30]. A noteworthy observation is the slightly lower rate of strength gain between 7 and 28 days (62% for M‑5.0 and 58% for M‑10, compared with 73% for M‑0.0). This suggests a mild retardation of primary cement hydration resulting from the initial dilution of the hydraulic binder, which partially counteracts the benefits of the filler effect. Consequently, at these low replacement levels, Ferrock behaves predominantly as an inert, high‑quality filler.

Zone 2: Peak Performance via Carbonation Binding (Mix M-15). This mixture represents the optimal performance threshold, attaining a 28‑day compressive strength of 46.4 MPa—a 25.4% increase over the control. This peak performance results from the carbonation reaction reaching its maximum efficacy. Foundational Ferrock studies employing microstructural analyses confirm that iron carbonate ($FeCO_3$) precipitates extensively throughout the capillary pore network and, crucially, reinforces the Interfacial Transition Zone (ITZ) between the paste and aggregates [11, 15]. Related Scanning Electron Microscopy (SEM) evidence indicates that the precipitated $FeCO_3$ forms a dense, interlocking microstructure that serves as pervasive micro‑reinforcement, effectively densifying the matrix and transforming it into a more monolithic and coherent composite [11]. At the 15% replacement level, an optimal balance is realized: sufficient Portland‑cement hydration furnishes a robust C‑S‑H gel skeleton, while the carbonation products derived from Ferrock actively reinforce and infill this framework without compromising its continuity.

Zone 3: Binder Dilution and Decline (Mixes M‑20 and M‑25). Beyond the 15% replacement threshold, the beneficial effects of Ferrock are offset by cement dilution—a well‑established principle in concrete science [26]. The compressive strength of mix M‑20 declines to 37.9 MPa (a marginal 2.4% gain relative to M‑0.0), while M‑25 drops to 35.0 MPa, representing a reduction of 2.0 MPa (5.4%) compared with conventional concrete. This decline occurs because Portland cement is a highly optimized hydraulic binder; replacing more than 15% of it substantially decreases the volume of clinker minerals (primarily tricalcium and dicalcium silicate) available to hydrate and form the continuous, strong, and cohesive calcium silicate hydrate (C‑S‑H) gel network that provides concrete's primary strength. Although the carbonation reaction persists and may even produce more iron carbonate ($FeCO_3$) in total, the resulting carbonate network is discontinuous. Without an adequate, continuous C‑S‑H matrix to serve as a host, the carbonate phase cannot establish an effective load‑bearing skeleton. Consequently, the overall structure weakens, as reflected in the Strength Efficiency Index (SEI) falling to 0.95 for M‑25. This outcome delineates the upper practical limit for Ferrock replacement in standard structural applications where compressive strength is a governing design criterion.

The observed non-linear relationship between strength and Ferrock content reflects a transition in the dominant microstructural mechanisms. At low replacement levels (5–10%), the fine Ferrock particles function primarily as micro-fillers, enhancing particle packing to densify the matrix and reduce porosity through a well-established physical filler effect [30]. The strength peak at 15% Ferrock indicates the threshold where carbonation binding becomes predominant, with iron carbonate ($FeCO_3$) precipitating extensively within pores and the Interfacial Transition Zone (ITZ) to form a stronger, more monolithic matrix, as supported by microstructural evidence [11]. Beyond this optimum, the strength reduction in M-20 and M-25 is attributed to the cement dilution effect, where excessive replacement diminishes the continuous, load-bearing C-S-H gel network from Portland cement hydration [7]; although carbonation continues, the discontinuous iron carbonate network cannot compensate for the weakened cohesive skeleton. This pattern of an optimal dosage aligns with findings for other novel supplementary cementitious materials (SCMs), and the 15% optimum identified here is significant because the achieved strength gain (25.4%) and Strength Efficiency Index (SEI=1.25) exceed typical values for conventional SCMs like fly ash at similar replacement levels [6-7], underscoring the substantial contribution of the carbonation mechanism.

### 3.1.2. Splitting Tensile Strength Analysis

The splitting tensile test results (Table 6), essential for evaluating cracking behavior, ductility, and long-term durability, exhibited a trend distinctly different from the compressive strength data. This divergence constitutes one of the most revealing characteristics of Ferrock's performance.

**Table 6. Splitting Tensile Strength Results**

| Mix ID | Ferrock (%) | Splitting tensile strength (MPa) | Increase vs. B1 | $f_{ct}/f_c^{/}$ | Toughness index (TI) |
|---|---|---|---|---|---|
| M-0.0 | 0 (Control) | 3.2 | Baseline (0%) | 0.124 | 1.00 |
| M-5.0 | 5 | 3.2 | 0% | 0.111 | 1.00 |
| M-10 | 10 | 3.4 | +6.3% | 0.110 | 1.06 |
| M-15 | 15 | 3.6 | +12.5% | 0.107 | 1.13 |
| M-20 | 20 | 3.7 | +15.6% | 0.128 | 1.16 |
| M-25 | 25 | 3.9 | +21.9% | 0.137 | 1.22 |

TI = (strength of Mix) / (strength of Control). A higher TI indicates greater tensile toughness.

In contrast to compressive strength, which peaked at 15% Ferrock (M-15) before declining, tensile strength demonstrated a consistent and progressive increase with higher Ferrock content. The M-25 mixture, containing 25% Ferrock, achieved a tensile strength of 3.9 MPa—a 0.7 MPa (21.9%) increase over the 3.2 MPa of the control mix (M-0.0). This contrasting behavior is not contradictory, but rather a direct outcome of the fundamental differences between compressive and tensile failure mechanisms, combined with the distinct micro-mechanical function of the precipitated iron carbonate.

Under compressive loading, the entire concrete matrix experiences uniform stress, leading to failure through the development of shear planes that fracture the microstructure. Compressive strength therefore depends critically on the cohesive integrity and continuity of the binding calcium silicate hydrate (C-S-H) gel matrix. Consequently, the cement dilution effect—where excessive Portland cement replacement weakens this continuous gel network—significantly reduces the compressive capacity of mixes M-20 and M-25.

In contrast, failure during a splitting tensile test results from the propagation of a single, dominant macro-crack. The force needed to advance this crack serves as an indicator of the material's fracture toughness. Within the concrete, the precipitated iron carbonate crystals function as numerous, randomly distributed microscopic anchors or barriers [15]. When a micro-crack forms and starts to grow, it is continually forced to alter its path, twist, bow around, and deflect against these hard, well-bonded particles. Each of these processes—deflection, bowing, and branching—demands considerable additional energy [31]. Thus, even in mix M-25, where the overall cementitious C-S-H matrix is weaker and less continuous, the extensive and dense network of iron carbonate crystals delivers exceptional, multi-faceted resistance to tensile crack propagation. The observed rise in tensile strength directly corresponds to the increased fracture energy needed to rupture the Ferrock-reinforced matrix.

### 3.1.3. Tensile-to-Compressive Strength Ratio

The tensile-to-compressive strength ratio ($f_{ct}$ / $f_c^{/}$) is a fundamental parameter in concrete technology and a primary indicator of material ductility versus brittleness. A higher ratio signifies reduced brittleness, reflecting a material's capacity for greater deformation and more pronounced warning signs prior to ultimate failure. The consistent and marked increase in this ratio—from 0.124 in the control mix (M-0.0) to 0.137 in M-25, representing an increase exceeding 10%—stands as one of the most pivotal findings of this investigation.

This increase in the tensile-to-compressive strength ratio carries substantial implications for structural design and safety. It demonstrates that although mix M-25 possesses a lower absolute compressive strength, a larger share of that strength can be mobilized to withstand tensile stresses prior to failure. Consequently, a structural component fabricated with M-25 would display markedly better crack control, enhanced energy absorption, and more detectable pre-collapse warnings—such as greater, safer deflections and more widespread micro-cracking—compared to conventional concrete (M-0.0), which may fail in a more abrupt, brittle fashion. This improved toughness and ductility are highly advantageous for enhancing the resilience of structures in seismic regions, for pavements enduring impact and fatigue, and for any application where long-term durability and safety are critical [32].

The observed trend of improved tensile performance and reduced brittleness aligns with direct fracture mechanics evidence from foundational studies on Ferrock-based systems. Research by Das et al. [15] on similar iron carbonate matrices has shown a substantial increase in fracture energy and toughness, where crack propagation is marked by significant deflection and bridging around the precipitated carbonate phases. The consistent, progressive enhancement in splitting tensile strength measured in this study at the structural concrete scale offers a direct macro-scale correspondence to this well-documented micro-mechanical toughening mechanism.

The consistent rise in tensile strength with increasing Ferrock content highlights its function as a toughness-enhancing modifier. This behavior originates from the fundamental distinction between failure mechanisms. Tensile failure, governed by crack propagation, is particularly influenced by microstructural barriers. The dispersed iron carbonate crystals serve as such barriers, deflecting and branching micro-cracks, which consumes additional fracture energy—a toughening mechanism well-documented for particle-reinforced composites [15, 31]. This accounts for the steady improvement in tensile performance. Furthermore, the increase in the tensile-to-compressive strength ratio from 0.124 to 0.137 signals a reduction in brittleness and an enhancement in ductility [32]. Structurally, this results in superior crack control, greater damage tolerance, and a more ductile failure mode—attributes that are especially valuable for seismic resistance and long-term durability [32]. From a practical standpoint, these findings support a performance-based approach to mix design: a 15% Ferrock replacement is optimal for applications requiring high compressive strength, while 20–25% replacement is advantageous for structural elements where flexural toughness and crack resistance are paramount.

## 3.2. Phase II

Expanding on the fundamental material properties identified in Phase I, Phase II of this research focused on a detailed evaluation of the structural-scale performance of RC-beams containing Ferrock as a partial cement substitute. The central aim was to connect material-level characteristics with full-scale structural response, particularly to assess how the previously reported gains in compressive and tensile strength, together with improved matrix toughness, influence real-world performance under flexural loading. This phase involved a thorough examination of crack development, failure modes, load-deflection behavior, and ultimate flexural capacity across six full-scale beams, each corresponding to a specific Ferrock content.

### 3.2.1. Cracking Behavior and Failure Modes

Figure 6 presents the complete crack propagation patterns recorded for all beams at ultimate failure. A close inspection of the cracking behavior demonstrated a strong and consistent effect of Ferrock on the fracture mechanics and damage tolerance of the concrete matrix. Every beam was carefully detailed with adequate shear reinforcement to promote a ductile flexural failure, a goal that was uniformly accomplished. The onset of cracking, identified by the first vertical flexural crack in the constant moment zone at the beam soffit, offered an initial, clear indication of Ferrock's influence. The load at first crack (*Pcrack*) correlated directly with the concrete's modulus of rupture and tensile strength, both of which changed appreciably with the amount of Ferrock.

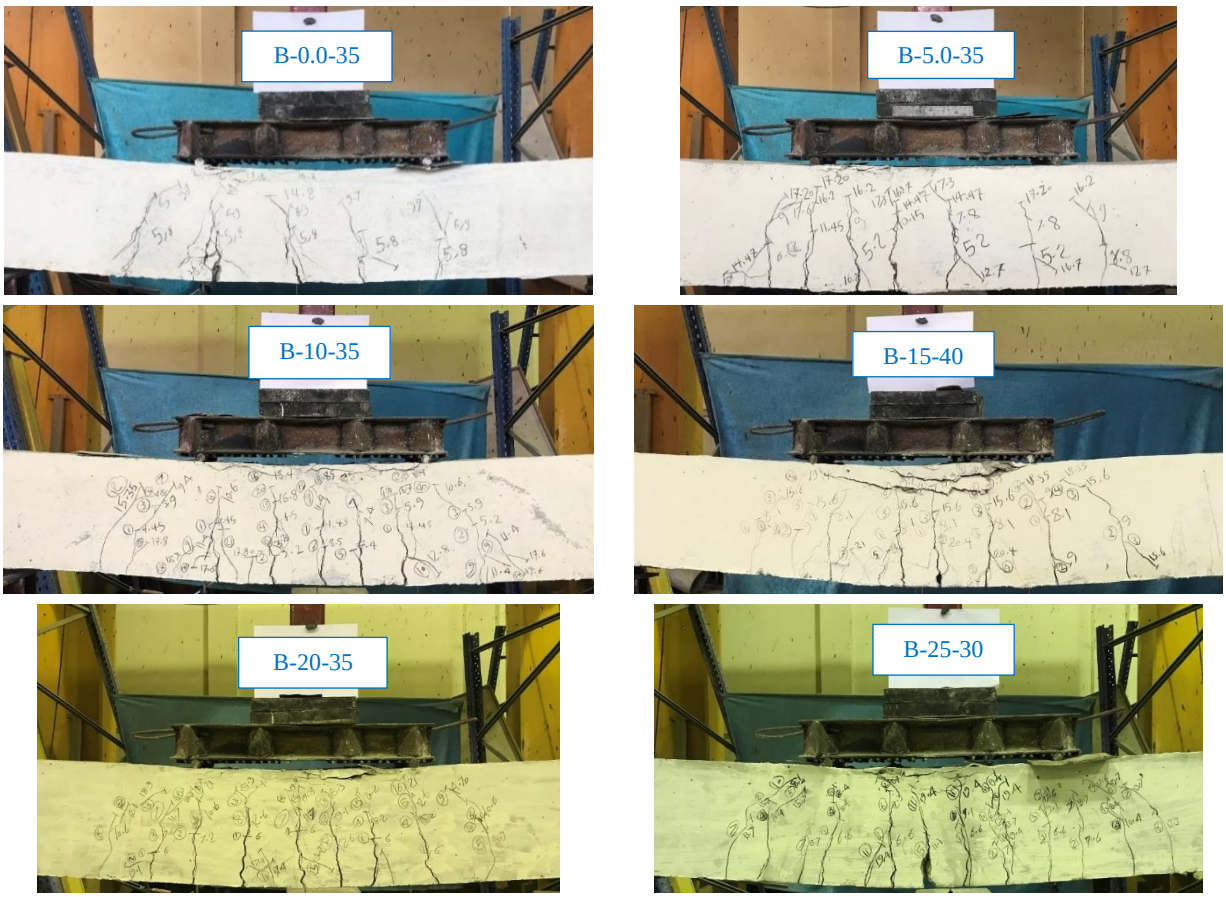


**Figure 6. Cracks and Failure Modes**

The control beam, B-0.0-35, which contained 0% Ferrock and had a splitting tensile strength of 3.2 MPa, developed its first crack at a load of 58 kN. By contrast, beam B-15-40, with 15% Ferrock and a tensile strength of 3.6 MPa, displayed a substantially higher resistance to crack initiation, with the initial crack forming at 82 kN—a 41.4% increase in cracking load. This improvement results directly from the denser, more uniform microstructure and the improved tensile characteristics imparted by the precipitation of iron carbonate. Beam B-25-30, possessing the highest tensile strength of 3.9 MPa, also performed well, cracking at 66 kN. Beams with lower Ferrock contents (B-5.0-35 and B-10-35) exhibited cracking loads comparable to or marginally lower than the control, suggesting that the beneficial microstructural influences become more pronounced above a replacement level of approximately 10%.

When the applied load exceeded the serviceability range, the post-cracking behavior of the beams diverged progressively. The control beam, B-0.0-35, formed a characteristic pattern of few, widely spaced flexural cracks that quickly widened and extended. In contrast, beams with higher Ferrock content—notably B-15-40, B-20-35, and B-25-30—displayed a distinctly improved crack pattern. These beams developed a greater number of finer, more closely spaced flexural cracks distributed along the constant moment region. Such a pattern is a clear and established sign of greater fracture energy and a tougher concrete matrix. The widespread network of iron carbonate crystals functioned as an effective micro-reinforcement, halting micro-cracks, diverting their progression, and hindering their merger into a single, dominant crack. This led to improved stress redistribution, enhanced bond with the steel reinforcement, and a more gradual accumulation of damage.

Each beam ultimately failed in a ductile flexural mode, the preferred failure mechanism for RC because it provides clear warning through substantial deflections and widespread cracking. The sequence of failure was consistent across all specimens: initial yielding of the tensile steel reinforcement, followed by crushing of the concrete in the compression zone at the beam's top. However, the qualitative progression of failure differed. Beams with higher Ferrock content (B-15-40, B-20-35, and B-25-30) exhibited a more extensive and distributed crack pattern, accompanied by a more gradual crushing of the compression zone. In contrast, failure in the control beam was comparatively more abrupt. The total absence of diagonal shear cracks in every beam verified the effectiveness of the shear design and definitively isolated flexural behavior as the focus of the investigation.

### 3.2.2. Load-Deflection Response and Stiffness

The load versus mid-span deflection curves, shown in Figure 7, offer detailed insight into each beam's structural stiffness, ductility, and energy absorption, enabling a direct comparison of their overall flexural behavior.

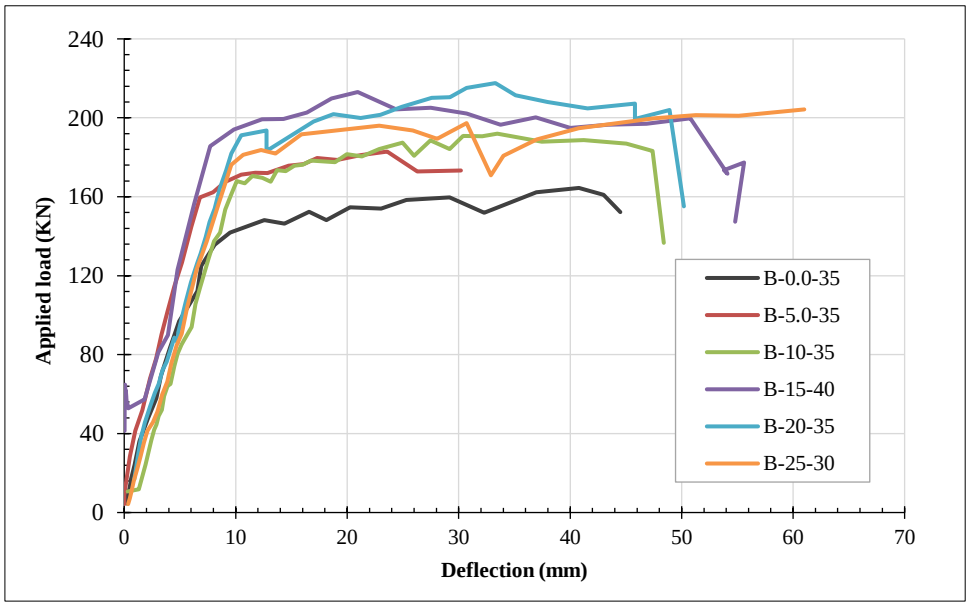


**Figure 7. Mid-Span Load-Deflection Curve**

The initial pre-cracking stiffness, reflected by the slope of the linear-elastic segment of the curves, was notably consistent across all beams. This implies that the static modulus of elasticity of the concrete—a property primarily determined by the type and proportion of aggregates and the composition of the paste—was not substantially changed by partially replacing cement with Ferrock. This outcome is particularly important for serviceability design, as it indicates that deflection calculations under service loads would not need adjustment for beams made with Ferrock concrete.

Post-cracking behavior, however, revealed distinct differences, as the stiffness reduction after initial cracking was less pronounced for beams with optimal Ferrock content. Beam B-15-40 (15% Ferrock) maintained the highest post-cracking stiffness, resulting from its superior matrix properties that enhanced "tension stiffening"—the ability of concrete between cracks to continue carrying tensile stress—which is particularly beneficial for controlling deflections under sustained service loads. The most revealing differences emerged in ductility and energy absorption, quantified by the area under the load-deflection curve; beam B-25-30 (25% Ferrock) exhibited the largest ultimate deflection of 47.5 mm, a 16.4% increase over the control beam's 40.8 mm, signifying a more ductile failure mode that provides a greater safety margin and more visible warning before collapse.

The total energy absorption, determined by the complete area under each load-deflection curve, was highest for the best-performing beams. Beam B-20-35 (20% Ferrock), which balanced elevated strength with favorable ductility, appears to have absorbed the greatest energy prior to failure. This dual attainment of high strength and high toughness is unusual for concrete and results directly from the distinctive micro-mechanical reinforcement imparted by the Ferrock.

### 3.2.3. Ultimate Failure Load

The ultimate failure load serves as the most decisive measure for evaluating the structural efficiency of the Ferrock-concrete beams. The results, detailed in Table 7, reveal a clear non-linear trend that echoes and intensifies the compressive-strength patterns identified in Phase I.

**Table 7. Cracking and Failure Parameters for the Beams**

| Beam ID | Cracking load, *Pcrack* (kN) | Increase in *Pcrack* vs. B-0.0-35 | Ultimate failure load, *Pmax* (kN) | Increase in *Pmax* vs. B-0.0-35 | Deflection at failure, (mm) | Failure mode |
|---|---|---|---|---|---|---|
| B-0.0-35 | 58 | Baseline | 164.0 | Baseline | 40.8 | |
| B-5.0-35 | 52 | -10.3% | 183.0 | +11.6% | 31.0 | |
| B-10-35 | 46 | -20.7% | 192.0 | +17.1% | 33.5 | Ductile flexure |
| B-15-40 | 82 | +41.4% | 213.0 | +29.9% | 21.0 | |
| B-20-35 | 60 | +3.4% | 217.6 | +32.7% | 33.3 | |
| B-25-30 | 66 | +13.8% | 204.0 | +24.4% | 47.5 | |

The control beam, B-0.0-35, failed at a load of 164 kN. A distinct improvement in performance is evident beginning with beam B-5.0-35, which withstood 183 kN—an increase of 11.6%. Beam B-10-35 attained a higher failure load of 192 kN, representing a 17.1% gain relative to the control. Peak structural performance was achieved by beams B-15-40 and B-20-35. Beam B-15-40 reached a failure load of 213 kN, a substantial 29.9% improvement, while beam B-20-35 attained the absolute maximum capacity of 217.6 kN, exceeding the control by 32.7%. This notable rise in flexural capacity directly reflects the 25.4% gain in cube compressive strength measured for the 15% Ferrock mix in Phase I. The increased load-carrying ability stems from a dual mechanism: a stronger compression zone that postpones concrete crushing, and a tougher tensile zone that retards the opening of major flexural cracks, enabling the tensile steel to yield fully and reach its ultimate strength.

The subsequent reduction in performance observed for beam B-25-30—which failed at 204 kN, a still-substantial 24.4% increase but below the capacities of B-15-40 and B-20-35—offers direct structural confirmation of the cement dilution effect noted in Phase I. At the 25% replacement level, the cohesive C-S-H gel matrix becomes deficient, ultimately capping the attainable flexural strength even though the beneficial effects on tensile toughness persist. This finding defines a clear, performance-based upper limit for Ferrock replacement in structural members where flexural capacity governs the design.

### 3.2.4. Comparison of Predicted and Experimental Flexural Capacities

Table 8 contrasts the experimentally determined flexural capacities of the beams with the predicted capacities derived from the American [33], Canadian [34], and European (EC2) [35] standards for steel-RC beams. The actual flexural capacity ($M_u$) was computed as $M_u = 0.6 \cdot P_{\max}/2$, consistent with the two-point loading configuration used in the tests, where $P_{\max}$ is the ultimate failure load of each beam.

**Table 8. Flexural Strength for the Beams**

| Beam ID | Standard | Flexural strength predicted by the standards, *Mn* (kN.m) | Actual strength, *Mu* (kN.m) | *Mu/Mn* |
|---|---|---|---|---|
| B-0.0-35 | ACI | 40.38 | 49.20 | 1.219 |
| B-5.0-35 | | 40.50 | 54.90 | 1.356 |
| B-10-35 | | 40.54 | 57.60 | 1.421 |
| B-15-40 | | 40.90 | 63.90 | 1.562 |
| B-20-35 | | 40.44 | 65.28 | 1.614 |
| B-25-30 | | 40.23 | 61.20 | 1.521 |
| B-0.0-35 | CSA | 40.23 | 49.20 | 1.223 |
| B-5.0-35 | | 40.36 | 54.90 | 1.360 |
| B-10-35 | | 40.40 | 57.60 | 1.426 |
| B-15-40 | | 40.75 | 63.90 | 1.568 |
| B-20-35 | | 40.30 | 65.28 | 1.620 |
| B-25-30 | | 40.09 | 61.20 | 1.527 |
| B-0.0-35 | EC2 | 40.38 | 49.20 | 1.219 |
| B-5.0-35 | | 40.50 | 54.90 | 1.356 |
| B-10-35 | | 40.54 | 57.60 | 1.421 |
| B-15-40 | | 40.90 | 63.90 | 1.562 |
| B-20-35 | | 40.44 | 65.28 | 1.614 |
| B-25-30 | | 40.21 | 61.20 | 1.522 |

For every beam, the measured flexural capacities were considerably higher than the values predicted by the design codes. The control beam (B-0.0-35, 0% Ferrock) had a predicted nominal moment of approximately 40.4 kN·m, whereas its measured capacity was 49.2 kN·m, giving an experimental-to-predicted ratio ($M_u/M_n$) of 1.22—22% above the code predictions. With the inclusion of 5% Ferrock (B-5.0-35), the measured moment increased to 54.9 kN·m while the predicted value remained at 40.4 kN·m, resulting in a $M_u/M_n$ ratio of about 1.36, or 36% higher than the code estimates. At 10% Ferrock (B-10-35), the measured capacity rose to 57.6 kN·m against a predicted 40.4 kN·m, yielding a ratio of 1.42, or 42% above the predicted strength.

The effect grew more marked at greater Ferrock contents. For the 15% replacement (B-15-40), the actual flexural capacity rose to 63.9 kN·m against a predicted strength of about 40.9 kN·m, corresponding to a ratio of 1.56 (56% higher). With 20% Ferrock (B-20-35), the measured strength reached a peak of 65.3 kN·m compared to a predicted 40.4 kN·m, producing the largest observed $M_u/M_n$ ratio of 1.62—62% above the code-based nominal prediction. Even at 25% Ferrock (B-25-30), the experimental strength remained notably elevated, measuring 61.2 kN·m against a predicted 40.2 kN·m, yielding a ratio of 1.52 (52% higher).

The overall trend confirms that incorporating Ferrock consistently raised the measured flexural capacity compared both to the control beam and to the predictions of all three design codes. Significantly, the greatest improvement occurred within the 15–20% Ferrock replacement range, implying that this interval may offer an optimal trade-off between cement reduction and strength enhancement.

Regarding the standards, the predicted values from ACI [33] and EC2 [35] were nearly identical for every beam, while the CSA [34] predictions were slightly lower (by less than 1%). These small discrepancies are insignificant when compared to the substantially larger strength increases attributable to the Ferrock addition. This result indicates that the selection of an international standard has a minimal effect on the predicted strength in these instances, whereas the material modification achieved through Ferrock is the decisive factor in enhancing capacity.

In summary, beams containing Ferrock consistently demonstrated greater flexural strength than predicted by the three design codes, with improvements ranging from 22% for the control specimen to over 60% for the beam with 20% Ferrock. These findings highlight the conservative character of code-based stress-block models and indicate that partially replacing cement with Ferrock—especially within the 15–20% range—can markedly enhance the flexural performance of reinforced concrete beams.

The demonstrated structural benefits—flexural capacities up to 33% higher and exceeding code predictions by as much as 62%—establish Ferrock as a sustainable material that also enhances performance. In contrast to traditional concretes with high volumes of supplementary cementitious materials (SCMs), which often exhibit slow strength development [6, 7], Ferrock mixtures displayed superior early-age and ultimate strength. Unlike certain geopolymers that necessitate complex mix designs [8, 9], Ferrock's partial replacement strategy allows simpler adoption within current industry practices while still providing substantial performance advantages. The significant over-strength relative to predictions from ACI 318 [33], CSA A23.3 [34], and Eurocode 2 [35] arises because code models do not incorporate the crack-arresting and micro-reinforcing contributions of the iron-carbonate network—a form of conservatism also observed for other advanced concretes [31, 32]. This underscores the importance of future research to develop adapted design guidelines that can safely utilize this enhanced efficiency. Importantly, these performance gains are achieved in parallel with Ferrock's carbon-negative lifecycle, which repurposes industrial waste and sequesters $CO_2$ during curing [12-14]. By simultaneously improving structural properties and lowering environmental impact, Ferrock addresses a central objective of sustainable construction: bridging the performance divide between conventional and environmentally friendly concretes [1, 4].

## 4. Conclusions

This investigation assessed the mechanical and structural performance of sustainable Ferrock concrete, in which Ordinary Portland Cement was partially replaced at different percentages with Ferrock—an iron carbonate-based binder largely derived from industrial by-products. The experimental program first determined the fundamental mechanical properties of several concrete mixtures, including compressive and splitting tensile strength, and then evaluated structural behavior via flexural tests on full-scale reinforced concrete beams. All specimens were fabricated, cured, and tested under controlled conditions using standardized methods to ensure repeatability. The beams were instrumented to record crack development, load-deflection response, and failure modes, delivering essential insights into the material's performance at both the material and structural scales. The following are the main conclusion points:

- A 15% Ferrock replacement level was established as the optimal proportion, producing a significant 25% gain in 28-day compressive strength. This maximum performance results from the highly efficient precipitation of iron carbonate, which fills pores and strengthens the critical Interfacial Transition Zone, yielding a denser and more monolithic matrix.
- Splitting tensile strength showed a steady, progressive increase, reaching a notable 22% improvement at the 25% replacement level. This outcome illustrates that Ferrock distinctively improves fracture toughness and energy absorption, because the dispersed iron carbonate crystals serve as microscopic barriers that deflect and impede crack growth.
- Structural performance was substantially improved, as full-scale reinforced beams with 20% Ferrock attained a notable 33% increase in ultimate flexural capacity. This confirms that the strength enhancements measured at the material level translate directly into superior real-world structural behavior, merging a stronger compression zone with a more resilient tensile zone.
- The inclusion of Ferrock markedly enhanced structural ductility and safety; one mixture exhibited a 16% larger ultimate deflection, signaling a more gradual and visibly warned failure progression. The steady increase in the tensile-to-compressive strength ratio verifies a fundamental decrease in material brittleness, a characteristic vital for seismic resilience and general structural safety.
- Crack resistance was substantially enhanced: the beam containing 15% Ferrock needed 41% greater load to produce the first flexural crack. In addition, this beam displayed a finer, more widespread crack distribution—a clear sign of a tougher matrix with improved stress redistribution and damage tolerance.
- Every Ferrock-concrete beam significantly surpassed the flexural capacity estimates of the major international design codes (ACI, CSA, and EC2), by as much as 62%. This outcome underscores the pronounced conservatism inherent in current code specifications and emphasizes Ferrock's potential to facilitate more efficient and higher-performance sustainable structural designs

## 5. Declarations

### 5.1. Author Contributions

Conceptualization, S.E., W.A., and A.G.; methodology, W.E., S.E., A.H., and A.M.; software, A.M., A.G., and W.A.; validation, S.E., W.A., and A.G.; formal analysis, W.E., A.H., and A.M.; investigation, A.M. and W.A.; resources, A.M. and I.A.; data curation, A.M. and W.A.; writing—original draft preparation, W.E., A.M., and A.H.; writing—review and editing, S.E., I.A., and A.G.; visualization, S.E., W.A., and I.A.; supervision, S.E., W.E., W.A., and A.G.; funding acquisition, I.A. All authors have read and agreed to the published version of the manuscript.

### 5.2. Data Availability Statement

The data presented in this study are available on request from the corresponding author.

### 5.3. Funding and Acknowledgments

The authors confirm that the data applied in this study is primary data and were generated at the building materials laboratory of the Faculty of Engineering at Mataria, Helwan University in cooperation with the College of Engineering and Design, Kingdom University, Bahrain. The authors would like to acknowledge that this research work was partially financed by Kingdom University, Bahrain from the research grant number KU-SRU-2024-05.

### 5.4. Conflicts of Interest

The authors declare no conflict of interest.

## 6. References

[1] Scrivener, K. L., John, V. M., & Gartner, E. M. (2018). Eco-efficient cements: Potential economically viable solutions for a low-CO2 cement-based materials industry. Cement and Concrete Research, 114, 2–26. doi:10.1016/j.cemconres.2018.03.015.

[2] Benhelal, E., Zahedi, G., Shamsaei, E., & Bahadori, A. (2013). Global strategies and potentials to curb CO2 emissions in cement industry. Journal of Cleaner Production, 51, 142–161. doi:10.1016/j.jclepro.2012.10.049.

[3] Imbabi, M. S., Carrigan, C., & McKenna, S. (2012). Trends and developments in green cement and concrete technology. International Journal of Sustainable Built Environment, 1(2), 194–216. doi:10.1016/j.ijsbe.2013.05.001.

[4] Damineli, B. L., Kemeid, F. M., Aguiar, P. S., & John, V. M. (2010). Measuring the eco-efficiency of cement use. Cement and Concrete Composites, 32(8), 555–562. doi:10.1016/j.cemconcomp.2010.07.009.

[5] Juenger, M. C. G., Winnefeld, F., Provis, J. L., & Ideker, J. H. (2011). Advances in alternative cementitious binders. Cement and Concrete Research, 41(12), 1232–1243. doi:10.1016/j.cemconres.2010.11.012.

[6] Rashad, A. M. (2013). A comprehensive overview about the influence of different additives on the properties of alkali-activated slag - A guide for Civil Engineer. Construction and Building Materials, 47, 29–55. doi:10.1016/j.conbuildmat.2013.04.011.

[7] Lothenbach, B., Scrivener, K., & Hooton, R. D. (2011). Supplementary cementitious materials. Cement and Concrete Research, 41(12), 1244–1256. doi:10.1016/j.cemconres.2010.12.001.

[8] Rihan, M. A. M., Onchiri, R. O., Gathimba, N., & Sabuni, B. (2024). Mechanical and Microstructural Properties of Geopolymer Concrete Containing Fly Ash and Sugarcane Bagasse Ash. Civil Engineering Journal (Iran), 10(4), 1292–1309. doi:10.28991/CEJ-2024-010-04-018.

[9] Adeleke, B. O., Kinuthia, J. M., Oti, J., Pirrie, D., & Power, M. (2024). Mechanical and Microstructural Investigation of Geopolymer Concrete Incorporating Recycled Waste Plastic Aggregate. Materials, 17(6), 1340. doi:10.3390/ma17061340.

[10] Das, S., Hendrix, A., Stone, D., & Neithalath, N. (2015). Flexural fracture response of a novel iron carbonate matrix – Glass fiber composite and its comparison to Portland cement-based composites. Construction and Building Materials, 93, 360–370. doi:10.1016/j.conbuildmat.2015.06.011.

[11] Das, S., Stone, D., Convey, D., & Neithalath, N. (2014). Pore- and micro-structural characterization of a novel structural binder based on iron carbonation. Materials Characterization, 98, 168–179. doi:10.1016/j.matchar.2014.10.025.

[12] Prashanth, M., Gokul, V., & Shanmugasundaram, M. (2019). Investigation on Ferrock Based Mortar an Environment Friendly Concrete. SSRN Electronic Journal, 1-4. doi:10.2139/ssrn.3461209.

[13] Puthoor, T. B. (2022). Introduction of sustainable and green materials in building construction for the wellness of the environment from an ethical and financial standpoint. Master Thesis, Technische Universität Wien, Vienna, Austria.

[14] Su, Q., Latypov, R., Chen, S., Zhu, L., Liu, L., Guo, X., & Qian, C. (2025). Life Cycle Assessment and Environmental Load Management in the Cement Industry. Systems, 13(7), 611. doi:10.3390/systems13070611.

[15] Das, S., Aguayo, M., Kabay, N., Mobasher, B., Sant, G., & Neithalath, N. (2018). Elucidating the influences of compliant microscale inclusions on the fracture behavior of cementitious composites. Cement and Concrete Composites, 94, 13–23. doi:10.1016/j.cemconcomp.2018.08.009.

[16] De Weerdt, K., Plusquellec, G., Belda Revert, A., Geiker, M. R., & Lothenbach, B. (2019). Effect of carbonation on the pore solution of mortar. Cement and Concrete Research, 118, 38–56. doi:10.1016/j.cemconres.2019.02.004.

[17] Rajesh, V., Patel, M., & Solanki, H. (2018). Development of carbon negative concrete by using Ferrock. Proceedings of the International Conference on Current Research Trends in Engineering and Technology, 26-27 April, 2018, Cochin, India.

[18] Deshpande, S., & Sakhare, V. (2024). Mechanical, microstructural, durability, and energy analysis of fly ash geopolymer modified with autoclaved aerated concrete block waste. Emergent Materials, 8(3), 2025–2044. doi:10.1007/s42247-024-00899-4.

[19] Mitikie, B. B., Gari, B. D., & Elsaigh, W. A. (2024). Ferrock cement and oxalic acid for enhanced concrete strength and durability against sulphate attack. Engineering Research Express, 6(2), 25122. doi:10.1088/2631-8695/ad592a.

[20] Singh, N., & Singh, J. (2025). Characterization of Concrete with Ferrock as a Potential Cement Substitute: Mechanical Strength, Durability and Microstructure analysis. Iranian Journal of Science and Technology - Transactions of Civil Engineering. doi:10.1007/s40996-025-01885-4.

[21] ES 4756-1. (2009). Cement Part:( 1) Composition, Specifications and Conformity Criteria for Common Cements. Egyptian Organization for Standardization and Quality (EOS), Cairo, Egypt. (In Arabic).

[22] BS EN 197-1:2011. (2011). Cement - Part 1: Composition, specifications and conformity criteria for common cements. British Standards Institution (BSI), London, United Kingdom.

[23] ASTM C618-19. (2019). Standard Specification for Coal Fly Ash and Raw or Calcined Natural Pozzolan for Use in Concrete. ASTM International, Pennsylvania, United States. doi:10.1520/C0618-19.

[24] ASTM C568/C568M-15. (2022). Standard Specification for Limestone Dimension Stone. ASTM International, Pennsylvania, United States. doi:10.1520/C0568_C0568M-15.

[25] ASTM C494/C494M-17. (2020). Standard Specification for Chemical Admixtures for Concrete. ASTM International, Pennsylvania, United States. doi:10.1520/C0494_C0494M-17.

[26] BS 5075-3:1985. (1985). Concrete admixtures - Specification for superplasticizing admixtures. British Standards Institution (BSI), London, United Kingdom.

[27] ASTM C39/C39M-21. (2008). Standard Test Method for Compressive Strength of Cylindrical Concrete Specimens. ASTM International, Pennsylvania, United States. doi:10.1520/C0039_C0039M-21.

[28] BS EN 12390-3:2019 - TC. (2019). Testing hardened concrete - Compressive strength of test specimens. British Standards Institution (BSI), London, United Kingdom.

[29] ASTM C496-96. (2017). Standard Test Method for Splitting Tensile Strength of Cylindrical Concrete Specimens. ASTM International, Pennsylvania, United States. doi:10.1520/C0496-96.

[30] Mehta, P. K., & Monteiro, P. J. (2006). Concrete microstructure, properties, and materials. McGraw-Hill, Columbus, United States.

[31] Shah, S. P., & Weiss, W. J. (2000). High performance concrete: strength, permeability, and shrinkage cracking. PCI/FHWA/FIB International Symposium on High Performance Concrete, 25-27 September, 2000, Orlando, United States.

[32] Aïtcin, P.-C. (1998). High Performance Concrete. CRC Press, London, United Kingdom.doi:10.4324/9780203475034.

[33] ACI CODE-318-25. (2025). Building Code for Structural Concrete—Code Requirements and Commentary (ACI CODE-318-25). American Concrete Institute (ACI), Farmington Hills, United States.

[34] CSA A23.3:24. (2024). Design of concrete structures. Canadian Standards Association (CSA), Toronto, Canada.

[35] EN 1992-1-1:2023. (2023). Eurocode 2: Design of concrete structures — part 1-1: General rules and rules for buildings, bridges and civil engineering structures. European Committee for Standardization (CEN), Brussels, Belgium.